Multiple phase transitions in CuO observed with thermal expansion

A. Rebello, Z. C. M. Winter, S. Viall, and J. J. Neumeier

Physics Department, P.O. Box 173840, Montana State University, Bozeman, Montana 59717-3840, USA

(Received 27 June 2013; published 16 September 2013)

High-resolution thermal-expansion measurements of single-crystalline CuO (tenorite) are reported for the temperature range $5 < T < 350$ K. The data reveal three transitions ($T_{N1} = 213$ K, $T_{N2} = 229.2$ K, and $T_{N3} = 229.8$ K), which corroborate the recently proposed magnetic phase diagram [Villarreal, Quirion, Plumer, Poirier, Usui, and Kimura, Phys. Rev. Lett. **109**, 167206 (2012)] revealing three distinct antiferromagnetic (AFM) phases. Analysis of the region surrounding T_{N2} and T_{N3} suggests that these phase transitions are continuous and yields estimates for the heat-capacity critical exponents of $\alpha_{T_{N2}} = 0.033(2)$ and $\alpha_{T_{N3}} = 0.040(9)$. Magnetic susceptibility measurements reveal spin-flop transitions at temperatures below T_{N1}, confirming that the b axis is the easy AFM axis.

I. INTRODUCTION

Transition-metal oxides exhibit exotic properties such as high-temperature superconductivity, spin and charge ordering, colossal magnetoresistance, and multiferroicity. Copper oxides, in particular, have been studied extensively due to the high superconducting transition temperatures of many compounds containing planar networks of copper-oxygen bonds.[1] Their magnetism and its relation to the superconducting state has been an important subtopic of study. The most simple copper oxide, CuO (tenorite), crystallizes with a monoclinic structure,[2] orders antiferromagnetically,[3] and is an electrical insulator with a gap possessing charge-transfer nature.[4] Ordering of charge domains was observed in CuO, similar to the type of ordering observed in the superconducting copper oxides.[5] The recent discovery[6] of spin-driven spontaneous electric-dipole ordering in CuO has created additional interest in CuO as a multiferroic oxide.[7–10]

Neutron diffraction[11–14] reveals the magnetic structure of CuO to consist of quasi-one-dimensional Cu chains along [1 0 $\bar{1}$]. Ordering results from superexchange coupling between Cu^{2+} orbitals along the [1 0 $\bar{1}$] crystallographic direction. The Cu-O-Cu bond angle of 146° plays a role in deciding the direction in which the magnetic moments order.[12] Two antiferromagnetic (AFM) phases[3,6] were discovered upon cooling: an incommensurate spiral ordering of the spins occurs at $T_{N2} = 229.3$ K (this transition is second order), followed by a first-order, commensurate, collinear ordering of the spins at $T_{N1} = 213$ K.

At T_{N2}, spontaneous polarization of the electric dipoles appears; below T_{N1}, it disappears. The direct transition from paramagnetic to spiral order, and the consequent induced multiferroic behavior, contradicted the general picture of ordering in other spin driven multiferroic materials like TbMnO$_3$,[15] MnWO$_4$,[16] and Ni$_3$V$_2$O$_8$.[17] In these materials, an intermediate incommensurate collinear antiferromagnetic transition appears between the paramagnetic phase and spiral ordered antiferromagnetic phase, and only the spiral magnetic order breaks the space inversion and induces ferroelectric order. However, theoretical studies based on Monte Carlo simulations[7,8] suggested that the direct transition from paramagnetic to the spiral magnetic ordering in CuO originates from the presence of a Dzyaloshinskii-Moriya-type coupling

between spin and lattice degrees of freedom. Another study using spin-only Landau-type free energy also supported the direct transition scenario in CuO, unlike other spin driven multiferroic materials.[9] Recently this issue was resolved when a third transition at $T_{N3} = 230$ K was observed using high-resolution ultrasonic velocity measurements;[18] this transition is a paramagnetic-incommensurate collinear magnetic phase transition.

Here, thermal-expansion measurements of single-crystalline CuO are reported. The data clearly corroborate transitions at $T_{N2} = 229.2$ K and $T_{N3} = 229.8$ K (with minor differences in temperature from Ref. 18). In addition, a distinct anomaly is observed near the first-order transition at $T_{N1} = 213$ K. Furthermore, thermodynamic analysis near T_{N2} and T_{N3} suggests that the phase transitions are continuous and yields estimates for the heat-capacity critical exponents of $\alpha_{T_{N2}} = 0.033(2)$ and $\alpha_{T_{N3}} = 0.040(9)$. Finally, magnetic measurements reveal a spin-flop transition at temperatures well below T_{N1}, confirming the b axis as the easy AFM axis in the commensurate collinear ordered state.

II. EXPERIMENTAL

Single crystals used in this work were grown with an optical image furnace using parameters similar to those reported in Ref. 6. The samples were oriented using Laue x-ray back reflection, and the images revealed good crystalline quality. Magnetic and heat-capacity measurements utilized a Quantum Design physical property measurement system. The thermal-expansion measurements were performed on a sample with dimensions 1.04, 0.98, and 1.11 mm in the reciprocal lattice axes a^*, b^*, and c^*, respectively. The asterisk symbol is omitted hereafter for simplicity. Measurements performed on a second sample yielded identical results. The quartz dilatometer[19] used for the measurements has 0.1-Å sensitivity to changes in length. The measurements along each axis consist of 19 000 data points. The linear thermal expansion (i.e., sample length change ΔL) is measured with a resolution of one part in 10^8, whereas the temperature is measured with a resolution of one part in 10^5. These differences lead to vertical scatter in the data when ΔL is differentiated with respect to temperature to obtain the thermal-expansion coefficient μ. The close temperature spacing in this particular experiment aggravates the scatter. To
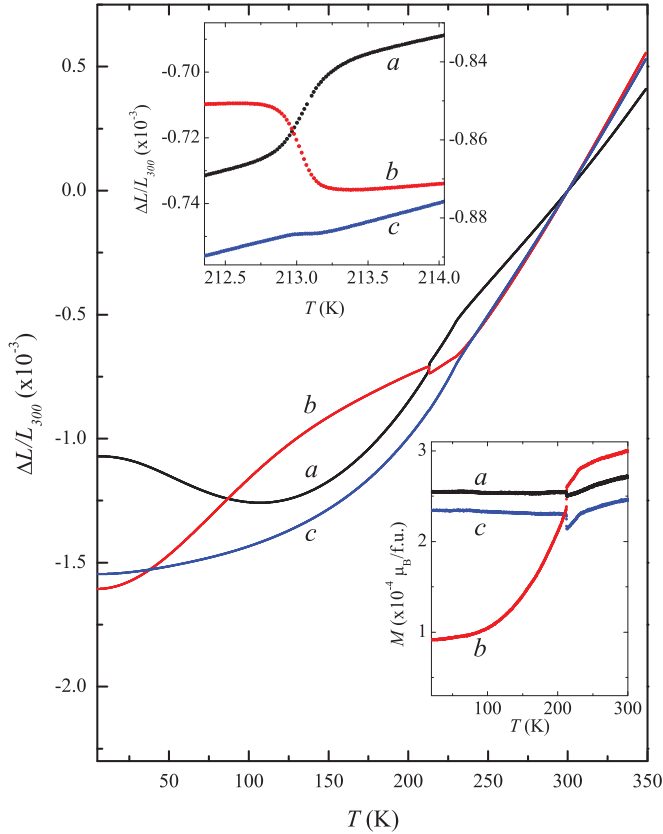
FIG. 1. (Color online) Temperature dependence of the linear thermal expansion ($\triangle L/L_{300}$) along the a, b, and c axes. Top inset: the expanded region near T_{N1}. Bottom inset: magnetization vs T along a, b, and c.

alleviate this problem, a piecewise Chebyshev fit of the $\triangle L$ data was performed prior to determining μ. Each fit region possessed a few degrees Kelvin of overlap with adjacent fit regions and was used to generate a new data set with equal spacing in temperature. This fitting procedure leads to an improved point-by-point derivative and can be viewed as smoothing of the data. The thermal-expansion coefficients derived from point-by-point temperature derivatives of raw and fit data were compared to be certain that no small features were overlooked and that the smoothed data are a valid representation of the raw data.

III. RESULTS AND DISCUSSION

The main panel of Fig. 1 shows the linear thermal expansion normalized to the length at 300 K, $\triangle L/L_{300}$, along the a, b, and c axes. It exhibits significant anisotropy. While the magnitude of the total variation of $\triangle L/L_{300}$ over the temperature range $5 < T < 300$ K along b and c is comparable, the change along a is smaller. Upon warming, $\triangle L/L_{300}$ along a exhibits a minimum near 125 K. Furthermore, $\triangle L/L_{300}$ along a and b shows remarkable changes in magnitude near the incommensurate spiral AFM to commensurate collinear AFM transition T_{N1} (213 K) (see top inset), where the sample dramatically contracts along a and expands along b at T_{N1} but exhibits only a moderate expansion along c. Expansion
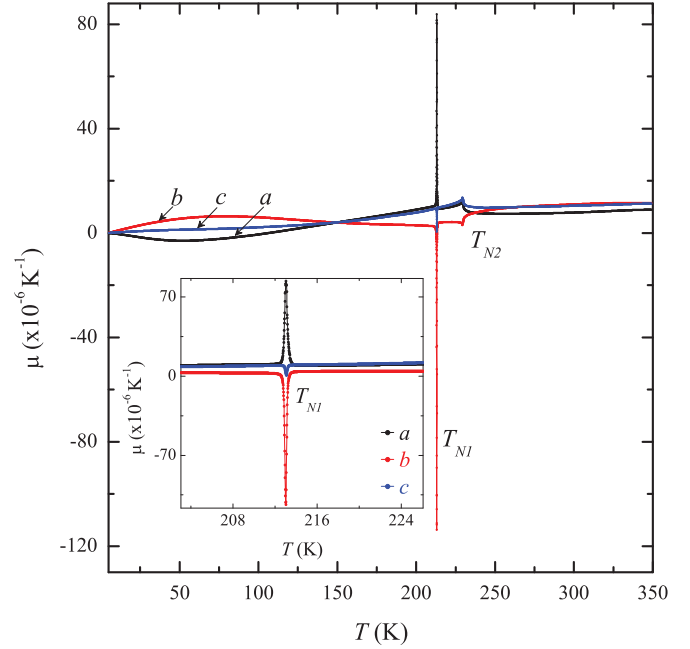
FIG. 2. (Color online) Temperature dependence of the linear thermal-expansion coefficient $\mu = (1/L_{300})\partial\triangle L/\partial T$ along the a, b, and c axes. Inset: the expanded region near T_{N1}.

in one direction along with contraction in another orthogonal direction can result from the Poisson effect.[20]

Crystallographic deformations may be observed near the Néel temperature in antiferromagnetic systems due to exchange striction, which implies a change in bond length due to magnetic ordering.[21,22] The exchange-coupling strength J is a function of distance between the magnetic atoms (r), and depending on the sign of dJ/dr the magnetic atoms will be pulled closer together or pushed further apart due to changes to the exchange interaction energy at the phase transition temperature, thus leading to lattice deformations. Hence, the observed large changes in $\triangle L/L_{300}$ near T_{N1} can be attributed to exchange striction. In addition, the distinct jumps in $\triangle L/L_{300}$ at T_{N1} signify that this phase transition is first order in nature. In contrast, no jumps are observed in $\triangle L/L_{300}$ in the vicinity of T_{N2}. Instead, changes of slope near T_{N2} can be seen in the upper inset of Fig. 1, suggesting that the phase transition is continuous (second order), with more subtle coupling to the lattice that requires additional analysis (see below). The temperatures where the changes in $\triangle L/L_{300}$ occur correlate well with the magnetization versus temperature shown in the lower inset of Fig. 1.

The linear thermal-expansion coefficient $\mu = (1/L_{300})\partial\triangle L/\partial T$ for the a, b, and c axes is presented in Fig. 2. Sharp anomalies in μ at T_{N1} are observed along all axes, due to the first-order nature of the transition. The anomalies along a and b are much larger than the anomaly along c (see inset of Fig. 2). Furthermore, very clear λ-like anomalies are observed in a, b, and c near 230 K, indicating the second-order nature of the transition [see Fig. 3 for more detail]. Though the magnitudes of the λ-like anomalies along the three axes are comparable, the direction of the feature along b is directed downward contrary to that along the other two axes, which are directed upward. Also, below ∼100 K,
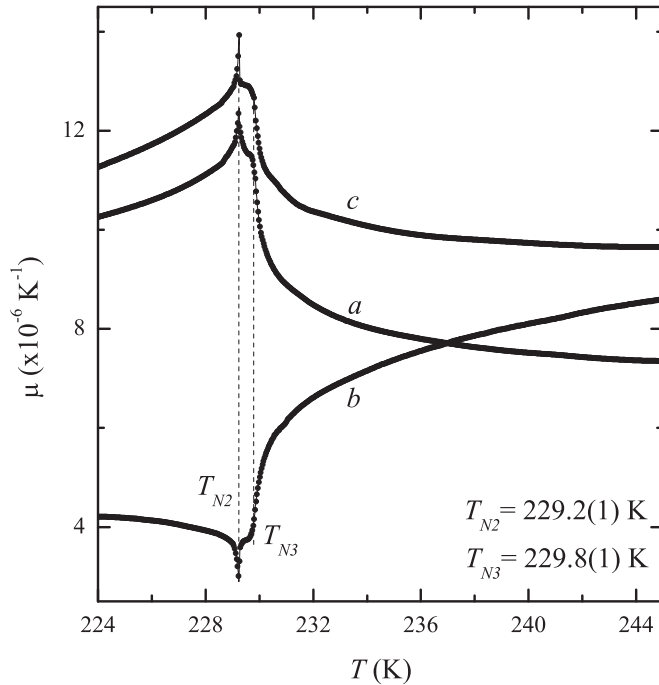
FIG. 3. Temperature dependence of the linear thermal-expansion coefficient $\mu = (1/L_{300})\partial \Delta L/\partial T$.

FIG. 4. Molar heat capacity after subtraction of the $T(\frac{\partial S}{\partial T})_N$ term from Eq. (1) (the result is called C_P^*) and $\lambda \Omega T$ plotted vs temperature.

μ along a shows a negative minimum, μ along b shows a positive maximum, and μ along c remains nearly constant. Negative thermal expansion is generally seen along specific directions in layered materials[23] due to the presence of anomalous phonon modes, making it possible that such modes are present in CuO at low temperatures. More interesting is the behavior of μ close to 230 K, where a double peak is observed along all axes. The peak in μ observed at 229.2 K clearly confirms the presence of the intermediate AFM phase revealed previously in high-resolution ultrasonic velocity measurements.[18] In this scenario, two order parameters are present near 230 K, one order parameter induces the paramagnetic-incommensurate collinear antiferromagnetic transition at $T_{N3} = 229.8$ K, which then couples to the other order parameter producing the complex spiral magnetic state at $T_{N2} = 229.2$ K.

The volume thermal-expansion coefficient Ω and C_P in the vicinity of T_{N2} and T_{N3} are now considered in some detail. According to the thermodynamics of a continuous phase transition, the heat capacity can be written as

$$C_P = T\left(\frac{\partial S}{\partial T}\right)_N + \upsilon T \Omega \left(\frac{\partial P}{\partial T}\right)_N. \qquad (1)$$

Here, S, P, υ, and Ω are the molar entropy, pressure, molar volume, and volume thermal-expansion coefficient, respectively; the subscript N signifies that Eq. (1) is valid near the Néel temperature.[24] When the entropy contribution is eliminated by subtracting the term that is linear in T from C_P, the result, C_P^*, is proportional to ΩT. For the region encompassing T_{N2} and T_{N3}, C_P^* scales with ΩT following a scaling relation[24] $C_P^* \simeq \lambda \Omega T$, as shown in Fig. 4. Satisfactory overlap is achieved for $\lambda = 3.0(1)\times 10^3$ J/mol K. The good overlap of the two data sets suggests that the phase transition

is continuous.[24] υ is calculated from the molar density at 300 K and $\Omega = (\mu_a + \mu_b + \mu_c)^*\sin\beta$ at 230 K. From x-ray data,[2] we took the value of β as $\sim 99.62°$. Using υ as 1.43×10^{-5} m^3/mol, the pressure derivative $dT_N/dP = 4.8(2)$ K/G Pa is obtained. Unfortunately, it is impossible to assign this pressure derivative to T_{N3} or T_{N2}, for reasons described below. A previous experimental study on the pressure dependence of the first-order transition in CuO has shown that T_{N1} decreases with increasing pressure at a rate of $dT_{N1}/dP = -2.9$ K/G Pa. However, the pressure dependence of T_{N2} could not be measured.[25] There is also no direct measurement of dT_{N3}/dP available for CuO at this time.

Noncollinear spin structures are known to play an important role in promoting electric polarization,[26] and significant coupling exists between the magnetic, lattice, and electronic components in systems exhibiting magnetoelectric behavior. Landau-type free-energy arguments have been applied to better understand the phase transitions in these systems and the influence of magnetic field on them.[18,27,28] These phenomenological treatments require the use of multicomponent order parameters where the electric polarization is implicitly included in the nonlocal formalism.[18,27] In the case of CuO, it is expected that the transition at T_{N2} would be continuous followed with another continuous phase transition at T_{N3}, through analogy[29] to multiferroic compounds such as[30] TbMnO$_3$. This is supported by our analysis using Eq. (1) and the data in Fig. 4. The wave vectors associated with the order parameters of these two phases can become locked to one another between the two transition temperatures.[29]

The interaction of the two order parameters in CuO is further complicated by the phase transition temperature separation of only 0.6 K. In practice, critical behavior is observed in magnetic systems[24,31] when the reduced temperature $t \equiv (T - T_N)/T_N$ is within the range $10^{-1} \lesssim |t| \lesssim 10^{-3}$. Thus,

for CuO it is certain that the region where the critical behavior associated with the phase transition at T_{N2} occurs extends well into the region of critical behavior associated with the phase transition at T_{N3} and vice versa. This consideration makes it clear that analysis of critical behavior associated with the phase transitions at T_{N2} and T_{N3} might be impossible or may yield critical exponents that are only estimates of the ideal values.

With this caveat in mind, analysis of the ΩT data is presented in the vicinity of the phase transitions T_{N2} and T_{N3}. Ideally, this analysis should yield the critical exponent α, which is normally referred to as the heat-capacity critical exponent.[24] The singularity in heat capacity (and ΩT) near a phase transition originates from a nonanalytic term in the thermodynamic free energy and can be asymptotically described by a function of the form

$$C_P^* = \left(\frac{A_\pm}{\alpha_\pm} \right) |t|^{-\alpha_\pm} + B_\pm + Dt, \qquad (2)$$

where $A_\pm$, $B_\pm$, and D are constants and $\alpha_\pm$ is the critical exponent.[24,31] The subscripts $+$ and $-$ for each parameter denote the values of the parameters above $(+)$ and below $(-)$ the phase transition temperature. Since C_P^* exhibits excellent overlap with $\lambda \Omega T$, Eq. (2) is an equally valid description of the singularity in $\lambda \Omega T$. Therefore, $\alpha_\pm$ can be extracted from the thermal-expansion data by plotting $\log(\lambda \Omega T - B_\pm - Dt)$ against $\log|t|$ and refining values for the fit parameters to obtain linear fittable ranges above and below the transition. Normally, the criterion $\alpha_+ \approx \alpha_-$ would imply that the transition is continuous. However, due to the adjacency of T_{N2} and T_{N3}, this condition might not hold.

Consider first analysis using $T_{N2} = 229.2(1)$ K, shown in the lower panel of Fig. 5. In this case, it was only possible to obtain an excellent linear range for $T < T_{N2}$. For this region, the value $\alpha_- = 0.033(2)$ was obtained with the fit parameters $D = 39(5)$ J/mol K, $B_+ = 14.4(3)$ J/mol K, and $B_- = 0.1(1)$ J/mol K. The range of linearity for $T > T_{N2}$ is good but clearly affected by the presence of T_{N3} and not nearly as convincing as the $T > T_{N3}$ fitting in the upper panel. From these observations, the critical exponent $\alpha_{T_{N2}} = 0.033(2)$ is identified with the transition at T_{N2}.

Consider next the top panel of Fig. 5, where the fitting utilizes T_{N3} as the critical temperature. The fit parameters are $D = 42(6)$ J/mol K, $B_+ = 6.3(7)$ J/mol K, and $B_- = 5.5(4)$ J/mol K, and $T_{N3} = 229.8(1)$ K. Careful inspection reveals that an excellent linear range is observed over more than two decades of t *only* for $T > T_{N3}$. This fit yields the critical exponent $\alpha_+ = 0.040(9)$. For $T < T_{N3}$ the quality of the fit is rather poor and clearly affected by the presence of T_{N2}; this fit yields $\alpha_- = 0.047(6)$. From these observations, the critical exponent $\alpha_{T_{N3}} = 0.040(9)$ is identified with the transition at T_{N3}.

Clearly, the results reveal that it is possible to observe critical behavior over a fairly large range of t below T_{N2} [with $\alpha_{T_{N2}} = 0.033(2)$] and above T_{N3} [with $\alpha_{T_{N3}} = 0.040(9)$]. The overlap of the two singularities means that the magnitudes of the obtained critical exponents should only be regarded as estimates of the ideal critical exponents associated with the order parameters responsible for each of the respective transitions. A difference between the obtained exponents would be expected since each is associated with a different
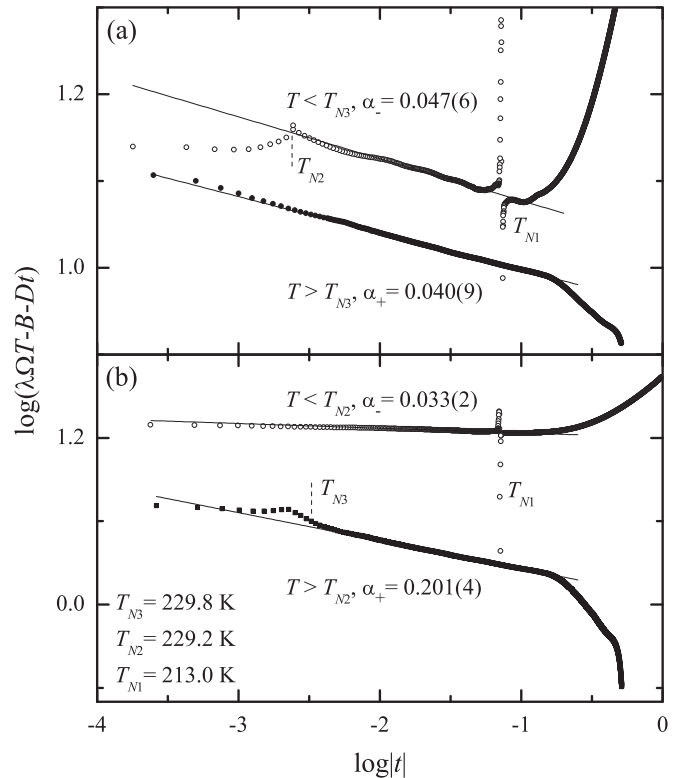
FIG. 5. Critical behavior of ΩT in the vicinity of T_{N2} and T_{N3}. The top panel shows the behavior if the transition temperature T_{N3} is used to calculate t, while the lower panel shows the behavior if T_{N2} is used. For easy reference, the transition temperatures are indicated on each of the curves.

order parameter. However, it appears that these two exponents are of similar magnitude and sign, within our uncertainty. Identification of these exponents with a specific universality class is difficult, since the majority of calculations of α involve ferromagnets, and few numerical calculations for antiferromagnets exist.[32] In the case of TbMnO$_3$, it was suggested that the low-temperature transition to the spiral AFM phase (similar to the transition at T_{N2}) should belong to the Ising universality class and the high-temperature transition to the collinear AFM phase (similar to the transition at T_{N3}) should belong to the XY universality class.[29] Calculations[33] for the ferromagnetic three-dimensional Ising model yield $\alpha = 0.125 \pm 0.015$, and Monte Carlo calculations for the ferromagnetic XY model[34] yield $\alpha = 0.1 \pm 0.14$. These values are provided for reference, but they illustrate that no definitive statements can be made by comparing our results to these values. Finally, we compare to experimental determinations of α for conventional antiferromagnets, which exhibit values for α of $0 < \alpha < 0.1$ (MnF$_2$), $-0.118(6)$ (NiO), $-0.15(6)$ (Co$_3$O$_4$), and $0.082(7)$ (CaMn$_2$O$_4$).[31,35–37]

As mentioned earlier, the magnetic structure of CuO is proposed to be collinear below 213 K. Collinear AFM systems possess an easy AFM axis, and neutron-diffraction studies have suggested[11–14] b as the easy axis in CuO. When a magnetic field is applied along the easy AFM axis for temperatures below T_N, a spin-flop (SF) transition can occur; it would be manifested as an abrupt jump in magnetization (M) at a critical magnetic field. This is due to the lowering
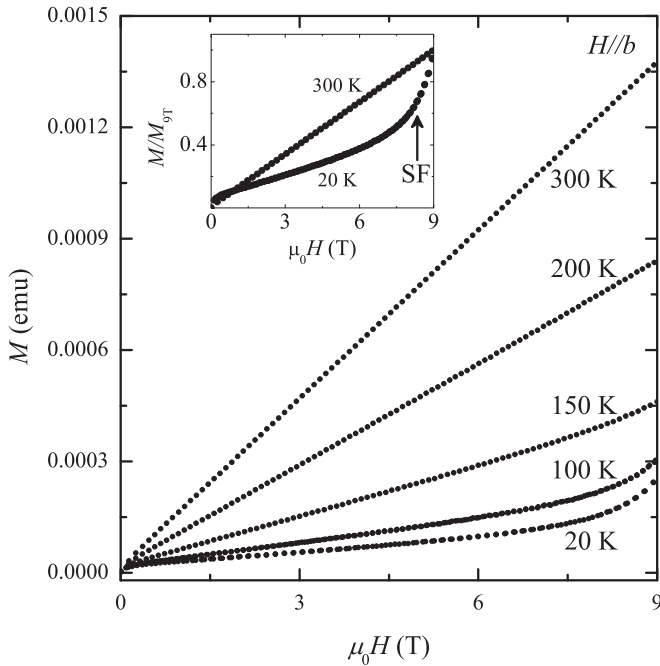
FIG. 6. Magnetization M vs magnetic field $\mu_0 H$ at the indicated temperatures. Inset: the normalized M vs $\mu_0 H$. The change of slope in M near 8 T provides evidence for a spin-flop (SF) transition.

of total energy in the SF configuration. A previous study[38] on polycrystalline powder CuO revealed a SF transition in CuO at ~10 T below 100 K and near 15 T at 200 K. In Fig. 6 similar measurements are shown on our single-crystalline specimen for H applied along b. In the paramagnetic region, M versus H is linear for H below 9 T. Similar linear behavior is observed at 150 and 200 K in the AFM state. Our magnetometer is limited to fields below 9 T, so we could not confirm the SF transition at 150 and 200 K. However, for 20 and 100 K our

data exhibit nonlinear behavior above 8 T due to the onset of a spin-flop transition; the inset of Fig. 6 shows this behavior on a vertical scale that is normalized to the magnetization at 9 T. This result is in good agreement with the previously reported critical-field value[38] in polycrystalline CuO at low temperatures. For the field applied along a and c, $M(H)$ remains linear at these temperatures (data are not shown here). Thus, these results confirm the collinear magnetic model in CuO at low temperatures with easy AFM axis along b.

IV. CONCLUSION

To summarize, the thermodynamic properties of single-crystalline CuO were investigated in the temperature range $5 < T < 350$ K. The thermal-expansion data provide sound evidence of three transitions in CuO ($T_{N1} = 213$ K, $T_{N2} = 229.2$ K, and $T_{N3} = 229.8$ K), which corroborates the recently proposed[18] magnetic phase diagram. Analysis of the region surrounding T_{N2} and T_{N3} suggests that the phase transitions are continuous and yields estimates for the heat-capacity critical exponents for T_{N2} and T_{N3} of $\alpha_{T_{N2}} = 0.033(2)$ and $\alpha_{T_{N3}} = 0.040(9)$, respectively. At present, these α values cannot be identified with specific universality classes. A pressure derivative for the phase transition region including T_{N2} and T_{N3} of $dT_N/dP = 4.6(2)$ K/GPa was obtained, but it is impossible to assign it to a specific transition temperature. Magnetic measurements reveal a spin-flop transition at temperatures well below T_{N1}, confirming the b axis as the easy AFM axis.

[1]M. Hücker, Physica C **481**, 3 (2012).

[2]H. Yamada, X.-G. Zheng, Y. Soejima, and M. Kawaminami, Phys. Rev. B **69**, 104104 (2004).

[3]E. Gmelin, U. Köbler, W. Brill, T. Chattopadhyay, and S. Sastry, Bull. Mat. Sci. **14**, 117 (1991).

[4]L. H. Tjeng, C. T. Chen, J. Ghijsen, P. Rudolf, and F. Sette, Phys. Rev. Lett. **67**, 501 (1991).

[5]X.-G. Zheng, C.-N. Xu, Y. Tomokiyo, E. Tanaka, H. Yamada, and Y. Soejima, Phys. Rev. Lett. **85**, 5170 (2000); X.-G. Zheng, C.-N. Xu, E. Tanaka, Y. Tomokiyo, H. Yamada, Y. Soejima, Y. Yamamura, and T. Tsuji, J. Phys. Soc. Jpn. **70**, 1054 (2001).

[6]T. Kimura, Y. Sekio, H. Nakamura, T. Siegrist, and A. P. Ramirez, Nat. Mater. **7**, 291 (2008).

[7]G. Giovannetti, S. Kumar, A. Stroppa, J. van den Brink, S. Picozzi, and J. Lorenzana, Phys. Rev. Lett. **106**, 026401 (2011).

[8]G. Jin, K. Cao, G.-C. Guo, and L. He, Phys. Rev. Lett. **108**, 187205 (2012).

[9]P. Toledano, N. Leo, D. D. Khalyavin, L. C. Chapon, T. Hoffmann, D. Meier, and M. Fiebig, Phys. Rev. Lett. **106**, 257601 (2011).

[10]V. Scagnoli, U. Staub, Y. Bodenthin, R. A. de Souza, M. Garcia-Fernandez, M. Garganourakis, A. T. Boothroyd, D. Prabhakaran, and S. W. Lovesey, Science **332**, 696 (2011).

[11]J. B. Forsyth, P. J. Brown, and B. M. Wanklyn, J. Phys. C **21**, 2917 (1988).

[12]B. X. Yang, T. R. Thurston, J. M. Tranquada, and G. Shirane, Phys. Rev. B **39**, 4343 (1989).

[13]P. J. Brown, T. Chattopadhyay, J. B. Forsyth, V. Nunez, and F. Tasset, J. Phys.: Condens. Matter **3**, 4281 (1991).

[14]M. Aïn, A. Menelle, B. M. Wanklyn, and E. F. Bertaut, J. Phys.: Condens. Matter **4**, 5327 (1992).

[15]T. Kimura, T. Goto, H. Shintani, K. Ishizaka1, T. Arima, and Y. Tokura, Nature (London) **426**, 55 (2003).

[16]G. Lawes, A. B. Harris, T. Kimura, N. Rogado, R. J. Cava, A. Aharony, O. Entin-Wohlman, T. Yildrim, M. Kenzelmann, C. Broholm, and A. P. Ramirez, Phys. Rev. Lett. **95**, 087205 (2005).

[17]K. Taniguchi, N. Abe, T. Takenobu, Y. Iwasa, and T. Arima, Phys. Rev. Lett. **97**, 097203 (2006).

[18]R. Villarreal, G. Quirion, M. L. Plumer, M. Poirier, T. Usui, and T. Kimura, Phys. Rev. Lett. **109**, 167206 (2012).

[19]J. J. Neumeier, R. K. Bollinger, G. E. Timmins, C. R. Lane, R. D. Krogstad, and J. Macaluso, Rev. Sci. Instrum. **79**, 033903 (2008).

[20]T. H. K. Barron and G. K. White, *Heat Capacity and Thermal Expansion at Low Temperatures* (Kluwer Academic, New York, 1999).

[21]S. Greenwald and J. S. Smart, Nature (London) **166**, 523 (1950).

[22]J. S. Smart and S. Greenwald, Phys. Rev. **82**, 113 (1951).

[23]A. Rebello, J. J. Neumeier, Z. Gao, Y. Qi, and Y. Ma, Phys. Rev. B **86**, 104303 (2012).

[24]J. A. Souza, Y.-K. Yu, J. J. Neumeier, H. Terashita, and R. F. Jardim, Phys. Rev. Lett. **94**, 207209 (2005).

[25]M. Ohashi, A. Tashiro, G. Oomi, E. Maeda, and X.-G. Zheng, Phys. Rev. B **73**, 134421 (2006).

[26]T. Kimura, J. C. Lashley, and A. P. Ramirez, Phys. Rev. B **73**, 220401 (2006).

[27]M. L. Plumer, Phys. Rev. B **78**, 094402 (2008); G. Quirion, M. L. Plumer, O. A. Petrenko, G. Balakrishnan, and C. Proust, *ibid.* **80**, 064420 (2009); S. G. Condran and M. L. Plumer, J. Phys. Condens. Matter **22**, 162201 (2010).

[28]V. P. Sakhnenko and N. V. Ter-Oganessian, Crystallography Rep. **57**, 112 (2012); J. Phys.: Condens. Matter **24**, 266002 (2012).

[29]A. B. Harris, A. Aharony, and O. Entin-Wohlman, J. Phys.: Condens. Matter **20**, 434202 (2008).

[30]K. Berggold, J. Baier, D. Meier, J. A. Mydosh, T. Lorenz, J. Hemberger, A. Balbashov, N. Aliouane, and D. N. Argyriou, Phys. Rev. B **76**, 094418 (2007).

[31]B. D. White, J. A. Souza, C. Chiorescu, J. J. Neumeier, and J. L. Cohn, Phys. Rev. B **79**, 104427 (2009).

[32]H. Kawamura, J. Phys. Soc. Jpn. **61**, 1299 (1992).

[33]M. E. Fisher, Rep. Prog. Phys. **30**, 615 (1967).

[34]W. Selke, J. Phys. C **13**, L261 (1980).

[35]D. T. Teaney, Phys. Rev. Lett. **14**, 898 (1965).

[36]L. M. Khriplovich, E. V. Kholopov, and I. E. Paukov, J. Chem. Theromodyn. **14**, 207 (1982).

[37]M. Massot, A. Oleaga, A. Salazar, D. Prabhakaran, M. Martin, P. Berthet, and G. Dhalenne, Phys. Rev. B **77**, 134438 (2008).

[38]O. Kondo, M. Ono, E. Sugiura, K. Sugiyama, and M. Date, J. Phys. Soc. Jpn. **57**, 3293 (1988).